DOI: 10.1002/adma.200600930

Cookie-like Au/NiO Nanoparticles with Optical Gas-Sensing Properties**

By *Giovanni Mattei, Paolo Mazzoldi, Michael L. Post, Dario Buso, Massimo Guglielmi,* and *Alessandro Martucci**

During the last 20 years, syntheses of nanoparticles with different sizes, shapes, compositions, and structures have been developed to create and study new nanomaterial properties.[1] For example, light emission from semiconductor quantum dots can be controlled by tailoring the size, size distribution, and surface states of the particles.[2] The optical properties of metal nanoparticles also depend on their size, size distribution, and morphology.[3] Different synthesis methods have been developed for preparing nanoparticles with a core/shell structure[4] (e.g., CdSe@ZnS or Au@SiO_2), or for controlling their morphological features (e.g., semiconductor rods,[5] stars or triangles,[6] and metal rods[7]), thus allowing the preparation of nanostructured materials with unique functional properties. In this paper we report for the first time the synthesis of "cookie"-like Au/NiO nanoparticles showing unique optical gas-sensor properties.

Films of NiO, a p-type semiconductor with a band gap of 4.2 eV, have been proposed as a sensitive material for chemoresistive[8] or optical[9] gas sensors. The working mechanism of these materials lies in a change of the electrical resistance or optical transmittance of the material caused by variations in the free-electron density, which in turn result from physisorption, chemisorption, and catalytic reactions between the probed gas and the surface of the material. The reaction with the target gas can be improved by either increasing the area of the reacting surface[10] or by doping the films with noble-metal nanoparticles[11]. The aim of this work is to synthesize nanoparticles possessing a metal oxide (NiO) and noble metal (Au) interface that is accessible to a target gas (CO). It has been reported earlier that the introduction of gold nanoparticles into metal oxide films is effective in enhancing or creating optical sensitivity to CO.[12] In the present work, Au/NiO nanoparticles have been embedded in a porous silica matrix with a high specific surface area, which increases the number of active sites for gas reaction and enhances sensor functionality.

The nanocomposites were prepared by the sol-gel technique. Thin films, with nominal molar ratios of $NiO/SiO_2 = 2:3$ and $NiO/Au = 5:1$, were deposited on SiO_2 glass and heated at 700 °C for 1 h in air. A film thickness of 525 nm has been evaluated from cross-section transmission electron microscopy (TEM) images. In a previous work,[13] we showed that NiO–SiO_2 nanocomposite films are still porous at 700 °C, and the porosity of the matrix provides a path for the gas molecules to reach the functional ultrafine particles embedded in the glass matrix.

In Figure 1a, we present a high-resolution TEM (HRTEM) image of a Au/NiO cookie-like nanocluster. Cross-section TEM measurements showed the presence of such clusters throughout the film thickness. Figure 1b shows a detail of the interface between Au and NiO at a higher magnification, from which the epitaxial growth at the interface can be clearly seen. Indeed, the Fourier transform (FT) of the HRTEM image (Fig. 1c) highlights the presence of two sets of parallel planes: the region with darker contrast in Figure 1b shows the lattice fringes of face-centered cubic (fcc) Au (111) planes (with interplanar distance $d(111) = 0.236$ nm), whereas a second smaller periodicity, arising from the region with brighter contrast in Figure 1b, can be indexed as originating from fcc NiO (200) planes ($d(200) = 0.207$ nm). A closer inspection of the HRTEM image shows, in the NiO part of the cluster, the presence of small amorphous zones superimposed on the crystalline regions. This result suggests a possible islandlike growth of the oxide, directed by the underlying Au template. It is interesting to highlight that we obtained a similar twofold coherent topology in studying the dealloying processes under thermal annealing for bimetallic Au–Cu nanoclusters in silica obtained by ion implantation,[14] where upon short annealing in an oxidizing atmosphere Au–Cu alloy nanoclusters were converted to an fcc Au-rich phase partially surrounded by a coherent fcc Cu_2O shell.

To further characterize the twofold composition of the cluster, we coupled scanning TEM (STEM) imaging with energy-dispersive X-ray spectroscopy (EDS) nanoanalysis. Figure 2 shows the STEM signal, collected with a high-angle annular

[*] Prof. A. Martucci, Dr. D. Buso, Prof. M. Guglielmi
Dipartimento di Ingegneria Meccanica–Settore Materiali
Università di Padova
Via Marzolo 9, 35131 Padova (Italy)
E-mail: alex.martucci@unipd.it
Prof. G. Mattei, Prof. P. Mazzoldi
Dipartimento di Fisica
Università di Padova
Via Marzolo 8, 35131 Padova (Italy)
Dr. M. L. Post
Institute for Chemical Process and Environmental Technology
National Research Council of Canada
1200 Montreal Road, Ottawa, ON K1A 0R6 (Canada)

[**] This work was supported by the Ministero Dell'Università e della Ricerca Scientifica (MURST) within a "Progetto di Ateneo n. CPDA042175" project of Padova University.

ADVANCED MATERIALS

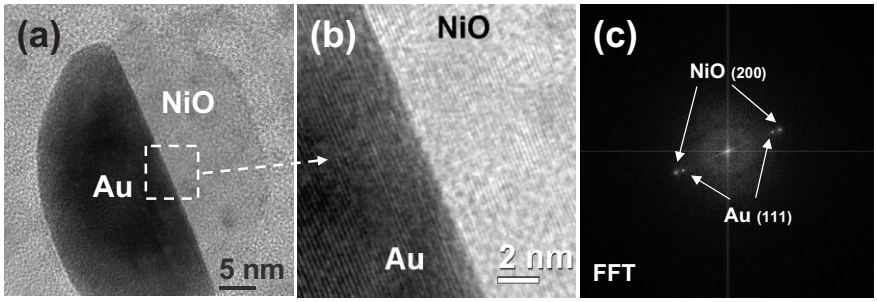

Figure 1. a,b) High-resolution TEM (HRTEM) images of the twofold Au/NiO cluster topology. c) Fourier transform (FT) of the HRTEM image in (b), showing the presence of two sets of parallel planes in Au and NiO.

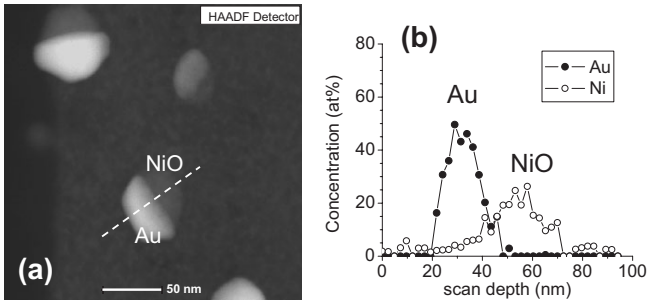

Figure 2. a) HAADF dark field STEM image of Au/NiO clusters. The white dashed line indicates the scan direction of the compositional EDS profile analysis shown in (b).

dark-field detector (HAADF), from a group of clusters. The brighter contrast in the image indicates the heavier element (Au in our case). By scanning a 1 nm (full width at half maximum; FWHM) electron probe on a single cluster (dashed line, Fig. 2a), we obtained by EDS the concentration profile reported in Figure 2b, which clearly indicates that the cluster consists of two parts: a Au region and a Ni-rich part. A correlation between Ni and O concentration profiles along the scan line was also observed (not shown in Fig. 2b), which is consistent with the presence of the NiO phase evidenced by the HRTEM and FT measurements (see Fig. 1c).

Data obtained in the HRTEM–STEM analyses have been used to model the optical absorption spectrum of the sample in the visible range. The experimental absorption curve is shown in Figure 3 and exhibits two main bands; the most intense band is centered at 613 nm and the other is a shoulder at about 530 nm.

To model both absorption bands, we redefined the unusual geometry of the twofold clusters in a way that is depicted in the inset of Figure 3, i.e., as a sum of spherical Au clusters (type 1 cluster) and a spherical core/shell structure (type 2 cluster) in which the Au core has the same size as the previous Au type and is surrounded by a shell of NiO. This two-component model is motivated and supported by the fact that the surface free electrons of Au experience direct dielectric coupling with the silica matrix from one side (type 1 cluster) and, on the opposite side, with the silica mediated by a thick shell of NiO (type 2 cluster). Therefore, by applying Mie theory, we simulated the experimental spectrum by adding the contribution of type 1 clusters, which have a surface plasmon resonance (SPR) band at 530 nm in silica, with that of type 2 clusters, which exhibit a red-shift of the Au SPR band induced by the higher dielectric constant (ε) of NiO ($\varepsilon_{NiO} = 5.4$) compared with that of silica ($\varepsilon_{SiO_2} = 2.13$), and account for the band at 613 nm. The agreement between the simulated and the experimental spectrum is quite satisfactory, as shown in Figure 3. It is worth noting that the numeric fitting procedure resulted in a 1:1 ratio between the population of type 1 and 2 clusters, again consistent with the assumption of the model. The spherical approximation used in the present model takes into account, in an average sense, the observed presence of prolate and oblate cookie-like structures. Moreover, the same strategy has successfully been applied in defining the optical absorption of similar partial core/shell Au-Cu_2O nanoclusters.[14,15] Comparable simulations made by assuming ellipsoidal cluster shapes did not give the same level of agreement. Hence, the principal result of the optical simulation is that the most intense absorption band is controlled by dielectric coupling at the Au/NiO interface, which red-shifts the position of the Au SPR band. This is important for explaining the results of the influence of gas absorption on the optical response of the material, as shown below.

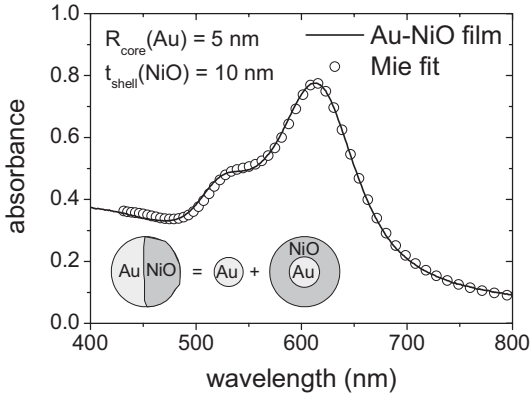

Figure 3. Experimental optical absorption spectrum of the sample (solid line) and corresponding effective medium fit (open circles) assuming a combination of monoelemental and core/shell nanoclusters. Absorbance is $\log_{10}$(incident light/transmitted light).

The gas sensing properties of the nanocomposite films were evaluated by measuring the variation of optical transmittance of the film when exposed to CO in air. The nanocomposite Au/NiO films exhibited clear and reversible absorbance changes in the vis-NIR wavelength region when exposed to CO, as shown in Figure 4. Upon exposure to 1 % CO, and

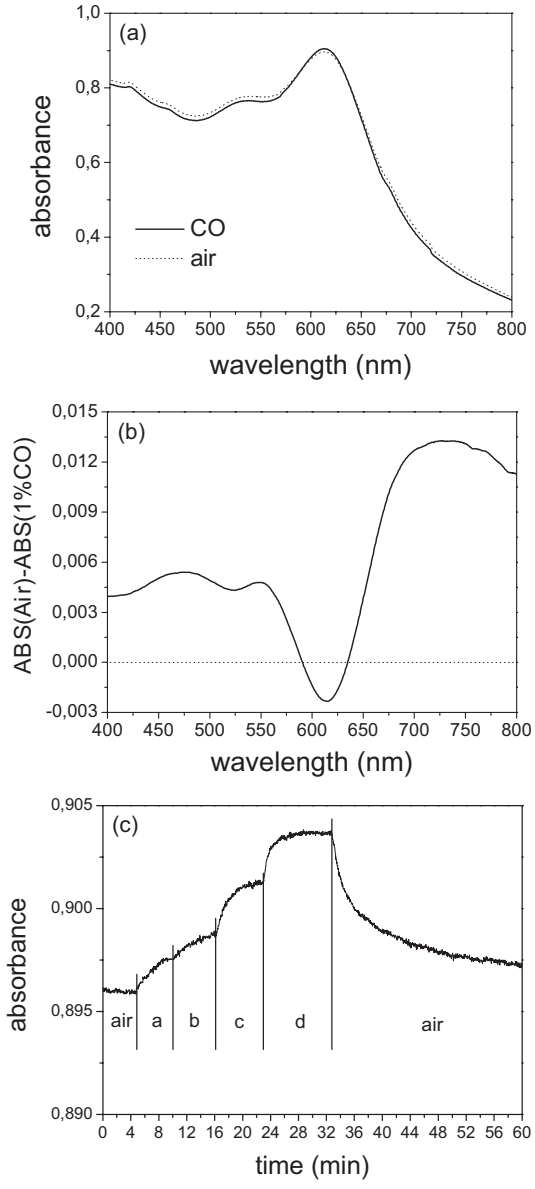

Figure 4. a) Absorption spectra of Au/NiO nanocomposite film in dry air (dotted line) and after exposure to 1 vol% CO (solid line). b) Absorbance in dry air minus absorbance in 1% CO (ΔA) of the Au/NiO nanocomposite film. c) Absorbance measured at 613 nm and different CO concentrations (a = 10, b = 100, c = 1000, d = 10 000 ppm) of the Au/NiO nanocomposite film. Absorbance is $\log_{10}$(incident light/transmitted light).

with the exception of wavelengths near the main plasmon absorption band around 613 nm, there is a decrease in absorbance over the whole wavelength range (Figure 4a). This feature can be better appreciated when considering the data showing the absorbance in air minus absorbance in 1% CO, defined as ΔA, reported in Figure 4b. The changes in absorbance clearly display a dependence in magnitude and sign of ΔA with respect to wavelength. Thus, in the region of most intense absorption, ($585 < \lambda < 635$ nm) there is a reversal of sign of the absorbance change (ΔA) in comparison with other wavelengths.

Similar behavior has been reported by Ando et al. for Co_3O_4 films containing Au nanoparticles exposed to H_2. However, that work reported only a positive ΔA for both Co_3O_4–Au and NiO–Au nanocomposite films when exposed to CO.[16,17] The present data is thus the first that provides evidence of negative ΔA in the plasmon wavelength region, which accompanies the exposure of nanoclusters with Au/NiO interfaces to CO. It is likely that the nanomorphology of the Au/NiO interface is intimately related to the existence of suppressed (or reversed) absorbance changes in the plasmon absorbance range.

In NiO films that have no noble-metal component, the decrease in absorbance is close to constant in the 350–850 nm wavelength range and is ascribed to a decrease in the positive hole density of NiO during catalytic oxidation of CO.[12] For the present case with NiO/Au, the decrease in absorbance at wavelengths outside the plasmon band can be ascribed to the same mechanism. The mechanism for the absorbance increase in the plasmon band is, however, not determined yet[16] but is clearly associated with the mediated catalytic oxidation of the reducing gas (CO). One possible explanation could be related to electron injection from NiO into Au in the cookie-like Au/NiO nanoparticles, thereby increasing the number of electrons available at the Au side of the Au/NiO interface that are involved in the catalytic oxidation of CO. This postulate is further supported considering that the variation in absorbance at 613 nm decreases as the CO concentration decreases (Fig. 4c). Further studies of the effect of bifurcation at a nanointerface on the key properties that influence the plasmon band (e.g., band position and width, permittivity, electrical conductivity, oxide species crystallite size) are required to ascertain the relative importance of the structural features presented here.

Experimental

The nanocomposites were prepared by mixing a matrix silica solution containing the precursors for silica and gold and a doping solution containing the precursor for NiO. The precursor solution for the silica matrix was made by mixing tetraethoxy silane (TEOS), methyl triethoxy silane (MTES), H_2O, and HCl in EtOH according to molar ratios TEOS:MTES:H2O:HCl:EtOH = 1:1:4:0.02:4. $HAuCl_4 \cdot 3H_2O$ was used as the metallic gold precursor and added directly in the matrix solution according to a Ni:Au = 5:1 molar ratio. The NiO precursor solution was made mixing $NiCl_2 \cdot 6H_2O$ in EtOH in the presence of N-[3-(trimethoxysilyl)propyl]-ethylenediammine (DAEPTMS) keeping the molar ratio of Ni:DAEPTMS = 1. The double amminic groups of DAEPTMS coordinate the Ni^{2+} cations in the solution while the silanic group ensures the homogeneous dispersion of cations distributed inside the final SiO_2 network. A nominal SiO_2:NiO molar ratio of 3:2 has been used. The two precursor sols were then mixed together to obtain the final batch [9b].

Films were deposited on quartz glass substrates via the dip-coating technique using a withdrawing speed of 100 cm min^{-1} at 23 °C and controlled relative humidity (RH = 25%). Thermal annealing of the films was performed in air at 700 °C for 60 min.

Structural and compositional characterization was performed at CNR-IMM (Bologna, Italy) on cross-sectional samples of the composite films. Measurements were taken with a field-emission FEI TECNAI F20 SuperTwin FEG-(S)TEM microscope operating at

ADVANCED MATERIALS

200 kV and equipped with an EDAX energy-dispersive X-ray spectrometer (EDS) for compositional analysis and a Gatan 794 Multiple Scan Camera, allowing digital image recording on a 1024×1024 pixel charge-coupled device (CCD) array. Scanning TEM (STEM) analysis coupled with EDS allowed compositional analysis on single clusters by means of line scans with an electron probe resolution of 1 nm FWHM.

Optical sensor functionality was studied by performing optical absorbance/transmittance measurements over the wavelength range $350 < \lambda < 800$ nm with sample films mounted on a heater in a custom built gas flow cell. Transmission data were recorded with a Varian Cary1E spectrophotometer with films heated at $T = 330\,^{\circ}\mathrm{C}$ (operating temperature) and for exposure to different CO concentrations in dry air. The substrate size for these measurements was approximately $1\ \mathrm{cm} \times 2\ \mathrm{cm}$ and the incident spectrophotometer beam was normal to the film surface and covering a $6\ \mathrm{mm} \times 1.5\ \mathrm{mm}$ section area.

Received: April 28, 2006
Revised: July 19, 2006
Published online: January 25, 2007

[1] Y. Yin, A. P. Alivisatos, *Nature* **2005**, *437*, 664.
[2] T. Trindade, P. O'Brien, N. L. Pickett, *Chem. Mater.* **2001**, *13*, 3843.
[3] C. Noguez, *Opt. Mater.* **2005**, *27*, 1204.
[4] F. Caruso, *Adv. Mater.* **2001**, *13*, 11.
[5] Y. Xia, P. Yang, Y. Sun, Y. Wu, B. Mayers, B. Gates, Y. Yin, F. Kim, H. Yan, *Adv. Mater.* **2003**, *15*, 353.
[6] A. G. Kanaras, C. Sonnichsen, H. T. Liu, A. P. Alivisatos, *Nano Lett.* **2005**, *5*, 2164.
[7] J. Perez-Juste, I. Pastoriza-Santos, L. M. Liz-Marzan, P. Mulvaney *Coord. Chem. Rev.* **2005**, *249*, 1870.
[8] I. Hotovy, J. Huran, P. Siciliano, S. Capone, L. Spiess, V. Rehacek, *Sens. Actuators, B* **2001**, *78*, 126.
[9] a) T. Kobayashi, M. Haruta, M. Ando, *Sens. Actuators, B* **1993**, *545*, 13. b) D. Buso, M. Guglielmi, A. Martucci, G. Mattei, P. Mazzoldi, C. Sada, M. L. Post, *Nanotechnology* **2006**, *17*, 2429.
[10] X. Wang, G. Sakai, K. Shimanoe, N. Miura, N. Yamazoe, *Sens. Actuators, B* **1997**, *45*, 141.
[11] M. Matsumiya, W. Shin, N. Izu, N. Murayama, *Sens. Actuators, B* **2003**, *93*, 309.
[12] M. Ando, T. Kobayashi, M. Haruta, *Catal. Today* **1997**, *36*, 135.
[13] A. Martucci, M. Pasquale, M. Guglielmi, M. Post, J. C. Pivin, *J. Am. Ceram. Soc.* **2003**, *86*, 1638.
[14] G. Mattei, G. De Marchi, C. Maurizio, P. Mazzoldi, C. Sada, V. Bello, G. Battaglin, *Phys. Rev. Lett.* **2003**, *90*, 085 502.
[15] G. Battaglin, E. Cattaruzza, C. Julián Fernández, G. De Marchi, F. Gonella, G. Mattei, C. Maurizio, P. Mazzoldi, A. Miotello, C. Sada, F. D'Acapito, *Nucl. Instrum. Methods Phys. Res. Sect. B* **2001**, *175*, 410.
[16] M. Ando, T. Kobayashi, S. Iijimac, M. Haruta, *J Mater. Chem.* **1997**, *7*, 1779.
[17] M. Ando, T. Kobayashi, M. Haruta, *J. Chem. Soc. Faraday Trans.* **1994**, *90*, 1011.

